Mathematical Geology, Vol. 32, No. 6, 2000

Understanding Anisotropy Computations[1]

Marian Eriksson[2] and Peter P. Siska[2]

Most descriptions of anisotropy make reference to reduced distances and conversion of anisotropic models to isotropic counterparts and equations are presented for a certain class of range-anisotropic models. Many descriptions state that sill anisotropy is modelled using a range-anisotropic structure having a very elongated ellipse. The presentations typically have few or no intervening steps. Students and applied researchers rarely follow these presentations and subsequently regard the programs that compute anisotropic variograms as black-boxes, the contents of which are too complex to try to understand. We provide the geometry necessary to clarify those computations. In so doing, we provide a general way to model any type of anisotropy (range, sill, power, slope, nugget) on an ellipse. We note cases in the literature in which the printed descriptions of anisotropy on an ellipse do not match the stated or coded models. An example is provided in which both range- and sill-anisotropic structures are fitted to the experimental variogram values from an elevation data set using the provided equations and weighted nonlinear regression. The original variogram values are plotted with the fitted surfaces to view the fit and anisotropic structure in many directions at once.

KEY WORDS: ellipse, nested structures, range, sill, slope, variogram.

INTRODUCTION

A number of books (Isaaks and Srivastava, 1989; Pannatier, 1996; Goovaerts, 1997; Myers, 1997) present the concept of geometric anisotropy using the reduced distance technique and “conversion to an isotropic model.” While not algebraically incorrect, this conversion process is confusing to most students and many practitioners, who rarely follow these presentations and subsequently regard the programs that compute anisotropic variograms as black-boxes, the contents of which are too complex to try to understand. The purpose of this paper is to help clarify the geometry behind and computations for anisotropy. For those needing a strong foundation in all aspects of variogram estimation, such an understanding is requisite. Those interested only in fitting variogram models, and who are neither interested in the interpretation of model parameters nor will have cause to code their own programs, can continue to rely on available programs. We will

[1]Received 9 December 1998; accepted 29 June 1999.
[2]Department of Forest Science, Texas A&M University, College Station, Texas, 77843-2135. e-mail: m-eriksson@tamu.edu

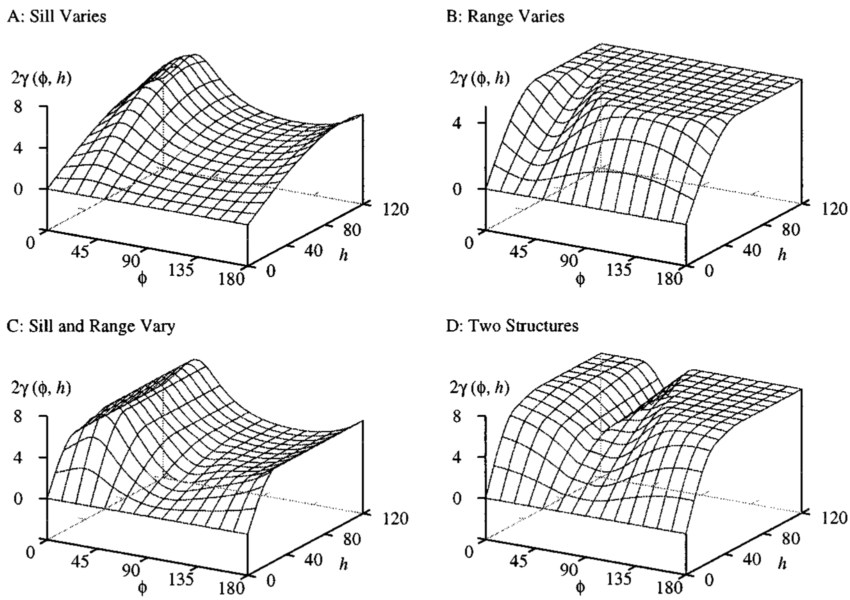

Figure 1. Examples of variograms with anisotropy; A, sill anisotropy in direction 30, B, range anisotropy in direction 30, C, sill in direction 30 and range anisotropy in direction 90, and D, nested range anisotropic structures in directions 90 and 150.

restrict ourselves to the two-dimensional case; extension to three dimensions is straightforward.

There are three concepts that are muddled together in the presentation by Isaaks and Srivastava (1989) of anisotropy—namely, geometric anisotropy, zonal anisotropy, and nested structures. Zimmerman (1993) further noted the inconsistent use, in the literature, of the terms geometric and zonal anisotropy. He suggested, instead, adopting the terms *nugget anisotropy, range anisotropy*, and *sill anisotropy*. Examples of range and sill anisotropies are shown for a spherical model in Figures 1A and 1B. In each case, the direction of the maximum, sill or range, is 30° north of east. Figure 1C combines range and sill anisotropies for a spherical model. The direction of maximum sill is 30° and the direction of maximum range is 90°. Complex variogram models are often constructed as the sum of simpler models. The simpler models are called nested structures. Figure 1D shows a variogram constructed as the sum of a spherical model with maximum range 100 in direction 90 and another spherical with maximum range 50 in direction 150. The axes in Figures 1A–1D are lag-distance h, angle of separation ϕ, and variogram value $2\gamma(h, \phi)$. We assume that angles are measured counterclockwise from east. Some variogram and Kriging implementations use angles measured in degrees azimuth (clockwise from north).

RANGE ANISOTROPY

Consider first the case of range anisotropy (Fig. 1B). It is assumed that the sill c of all directional variograms is the same. The basic idea behind most anisotropic modeling algorithms is that there is some separation direction θ in which the directional variogram has maximum range $a_{\max}$. Perpendicular to that direction, $\theta \pm \pi/2$, the range is assumed to be minimum, $a_{\min}$. The maximum and minimum ranges define an ellipse (Fig. 2) that lies in the $(\Delta x, \Delta y)$ coordinate system, where x and y denote the rectangular locational coordinates, usually eastings and northings. That is, Δx is the lag distance in the x direction and Δy is the lag distance in the y direction. The range a_ϕ of the directional variogram for any separation angle ϕ is assumed to lie on the ellipse.

Let u and v represent coordinates in a system oriented along the major and minor axes of the ellipse. Then the equation of the ellipse is

$$(u/a_{\max})^2 + (v/a_{\min})^2 = 1 \tag{1}$$

We can convert the rectangular uv coordinates to and from polar coordinates via the relationships

$$a_\xi = \sqrt{u^2 + v^2} \qquad u = a_\xi \cos \xi$$
$$\xi = \tan^{-1}(v/u) \qquad v = a_\xi \sin \xi$$

where ξ is the angle of separation relative to the uv coordinate system and a_ξ is the range in that direction (Fig. 2).

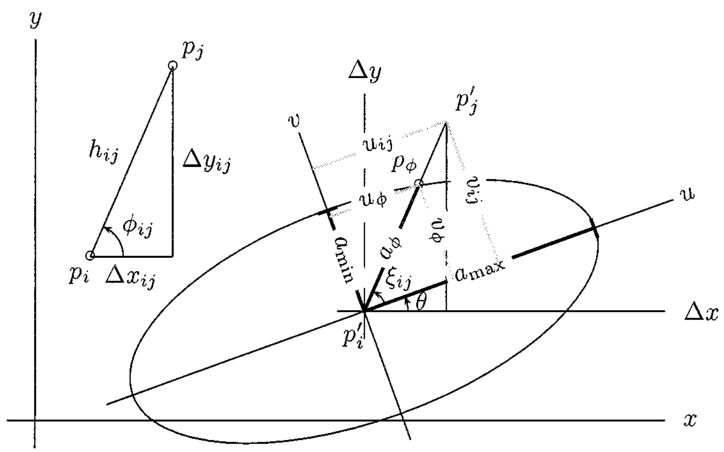

Figure 2. Geometry of a range-anisotropic ellipse as it relates to points p_i and p_j separated by distance h_{ij} in the direction ϕ_{ij}. The range in direction ϕ_{ij} is $a_{\phi_{ij}}$.

Rather than directly specifying $a_{\max}$ and $a_{\min}$, most implementations of variogram modeling require that the user specify the magnitude a of *either* maximum or minimum anisotropy, and a factor η that relates a to $a_{\max}$ and to $a_{\min}$. If $\eta > 1$, then $a_{\min} = a$ and $a_{\max} = \eta a$. Similarly, if $\eta < 1$, then $a_{\max} = a$ and $a_{\min} = \eta a$. For concreteness assume, for now, that $\eta < 1$.

Upon substituting into (1) we see that the ellipse can be represented as

$$\frac{a_\xi^2 \cos^2 \xi}{a^2} + \frac{a_\xi^2 \sin^2 \xi}{(a\eta)^2} = 1 \tag{2}$$

and that the range in direction ξ, relative to the uv coordinate system, is

$$a_\xi = a\eta \Big/ \sqrt{\eta^2 \cos^2 \xi + \sin^2 \xi} \tag{3}$$

Now consider two points p_i and p_j having locational coordinates (x_i, y_i), (x_j, y_j), and translate the two points to the origin p_i' of the ellipse (Fig. 2). The separation distance is $h_{ij} = \sqrt{\Delta y_{ij}^2 + \Delta x_{ij}^2}$ and the separation angle, relative to the $\Delta x \Delta y$ coordinate system, is $\phi_{ij} = \tan^{-1}(\Delta y_{ij}/\Delta x_{ij})$. Relative to the uv coordinate system the separation angle is $\xi_{ij} = \phi_{ij} - \theta$. From (3), the range in direction ϕ_{ij} is

$$a_{\phi_{ij}} = a_{\max} a_{\min} \Big/ \sqrt{a_{\min}^2 \cos^2(\phi_{ij} - \theta) + a_{\max}^2 \sin^2(\phi_{ij} - \theta)}$$

or using the anisotropy ratio,

$$a_{\phi_{ij}} = a\eta \Big/ \sqrt{\eta^2 \cos^2(\phi_{ij} - \theta) + \sin^2(\phi_{ij} - \theta)} \tag{4}$$

The ij subscripting is used to emphasize the fact that these distances and angles are defined by, and calculated for, the pair of points p_i and p_j.

The range parameter, usually symbolized as a in an isotropic variogram equation, can be replaced by Equation (4) to obtain an anisotropic variogram model. Figure 1B, for example, was created simply by plotting

$$2\gamma(h, \phi) = \begin{cases} 5\left(1.5\left(\frac{h\sqrt{0.3^2 \cos^2(\phi - 30) + \sin^2(\phi - 30)}}{100 \cdot 0.3}\right) - 0.5\left(\frac{h\sqrt{0.3^2 \cos^2(\phi - 30) + \sin^2(\phi - 30)}}{100 \cdot 0.3}\right)^3\right) \\ \qquad \text{for } h \leq 100 \cdot 0.3/\sqrt{0.3^2 \cos^2(\phi - 30) + \sin^2(\phi - 30)} \\ 5 \qquad \text{otherwise.} \end{cases}$$

The sill is $c = 5$, the range, in direction $\theta = 30$, is $a_{\max} = 100$, the anisotropy ratio is $\eta = 0.3$, so the minimum range, in direction 120, is $a_{\min} = 30$. Notice that the anisotropic variogram model is formally a function of both lag distance h and separation angle ϕ.

Making Sense of the Reduced Distance Approach

As in the previous example of creating Figure 1B, Equation (4) can be used directly in the calculation of variogram values. However, most authors and algorithms use the reduced distance and standardized model approach. One could, of course, begin with Equation (4) to obtain the computational algorithm as presented, for example, by Isaaks and Srivastava (1989) or Goovaerts (1997), but it is more instructive to take another look at the geometry.

Step 1

The uv coordinate system is related to the $\Delta x \Delta y$ coordinate system via the rotation matrix

$$\boldsymbol{R} = \begin{bmatrix} \cos\theta & \sin\theta \\ -\sin\theta & \cos\theta \end{bmatrix}$$

Again translate the two points p_i and p_j to the center of the anisotropy ellipse such that p_i' coincides with the center, and apply the rotation matrix to p_j':

$$\begin{bmatrix} u_{ij} \\ v_{ij} \end{bmatrix} = \begin{bmatrix} \cos\theta & \sin\theta \\ -\sin\theta & \cos\theta \end{bmatrix} \begin{bmatrix} \Delta x_{ij} \\ \Delta y_{ij} \end{bmatrix} \tag{5}$$

Step 2

The intersection of line $v = (v_{ij}/u_{ij})u$, defined by points p_i' and p_j', with the ellipse defines the point $p_{\phi_{ij}}$ having distance $a_{\phi_{ij}}$ from the center of the ellipse. So substituting $v = (v_{ij}/u_{ij})u$ into the Equation (1) of an ellipse, we find that

$$\frac{u^2}{u_{ij}^2}\left(\frac{u_{ij}^2}{a_{\max}^2} + \frac{v_{ij}^2}{a_{\min}^2}\right) = 1$$

Solving for u and substituting into the equation of the line gives

$$u_{\phi_{ij}} = u_{ij} \Bigg/ \sqrt{\frac{u_{ij}^2}{a_{\max}^2} + \frac{v_{ij}^2}{a_{\min}^2}}$$

and

$$v_{\phi_{ij}} = v_{ij} \Bigg/ \sqrt{\frac{u_{ij}^2}{a_{\max}^2} + \frac{v_{ij}^2}{a_{\min}^2}}$$

Subscripts have been added to u and v to emphasize the fact that these are the uv coordinates of the point $p_{\phi_{ij}}$ on the ellipse at separation angle ϕ_{ij}.

Noting that $\sqrt{u_{ij}^2 + v_{ij}^2} = \sqrt{\Delta x_{ij}^2 + \Delta y_{ij}^2} = h_{ij}$ and using the definitions of $u_{\phi_{ij}}$ and $v_{\phi_{ij}}$, the range in direction ϕ_{ij} is found to be

$$a_{\phi_{ij}} = \sqrt{u_{\phi_{ij}}^2 + v_{\phi_{ij}}^2} = h_{ij} a_{\max} a_{\min} \Big/ \sqrt{\left(a_{\min}^2 u_{ij}^2 + a_{\max}^2 v_{ij}^2\right)} \tag{6}$$

This is a reexpression of Equation (4) based on the rotated coordinates. Another useful expression for $a_{\phi_{ij}}$ in terms of the original coordinates is

$$a_{\phi_{ij}} = h_{ij} \Big/ \sqrt{b_1 \Delta x_{ij}^2 - b_2 \Delta x_{ij} \Delta y_{ij} + b_3 \Delta y_{ij}^2} \tag{7}$$

where $b_1 = (\cos\theta / a_{\max})^2 + (\sin\theta / a_{\min})^2$, $b_2 = 2\sin\theta\cos\theta(1/a_{\min}^2 - 1/a_{\max}^2)$, and $b_3 = (\sin\theta / a_{\max})^2 + (\cos\theta / a_{\min})^2$. This is, essentially, the form used by Zimmerman (1993) in his Equation (8).

Step 3

A number of the common variogram models incorporate the range as the divisor in the ratio $h'_{ij} = h_{ij} / a_{\phi_{ij}}$. This term is referred to as the reduced distance. From (6) it is clear then that

$$h'_{ij} = \sqrt{\frac{u_{ij}^2}{a_{\max}^2} + \frac{v_{ij}^2}{a_{\min}^2}} \tag{8}$$

The reduced distances can be used directly in the Gaussian, spherical, and exponential variogram models. For example, Figure 1B can be generated by using the rotation matrix $\boldsymbol{R}$ to convert $(\Delta x, \Delta y)$ coordinates to (u, v) coordinates and then plotting

$$2\gamma(h, \phi) = \begin{cases} 5\left(1.5\sqrt{(u/100)^2 + (v/30)^2} - 0.5\left(\sqrt{(u/100)^2 + (v/30)^2}\right)^3\right) \\ \qquad \text{for } h \le \sqrt{\frac{u^2 + v^2}{(30u)^2 + (100v)^2}} \\ 5 \qquad \text{otherwise.} \end{cases}$$

Combining the Steps

The computations leading to h'_{ij} can be combined as follows:

$$\begin{bmatrix} u'_{\phi_{ij}} \\ v'_{\phi_{ij}} \end{bmatrix} = \begin{bmatrix} 1/a_{\max} & 0 \\ 0 & 1/a_{\min} \end{bmatrix} \begin{bmatrix} \cos\theta & \sin\theta \\ -\sin\theta & \cos\theta \end{bmatrix} \begin{bmatrix} \Delta x_{ij} \\ \Delta y_{ij} \end{bmatrix}$$

and $h'_{ij} = \sqrt{(u'_{\phi_{ij}})^2 + (v'_{\phi_{ij}})^2}$. This is the computational form presented by Isaaks and Srivastava (1989) and repeated by Myers (1997). It differs from Goovaerts (1997) only in that he assumed that angles were measured clockwise from the north and used the relationships between a, η, $a_{\max}$, and $a_{\min}$, rather than $a_{\max}$ and $a_{\min}$, themselves. Journel and Huijbregts (1978) actually rotate back to the $\Delta x \Delta y$ orientation before computing the "reduced distances," but that reorientation is unnecessary.

Many authors (e.g., Isaaks and Srivastava 1989; Pannatier, 1996; Goovaerts, 1997; Myers, 1997; Deutsch and Journel, 1998) state, effectively, that the above computations are equivalent to a rotation of axes, followed by the reduction of the separation distance to h'_{ij}, which allows the use of an isotropic model. This is misleading. It is true that, *given* ϕ_{ij}, the use of $h'_{ij} = h'_{ij}/1$ in place of the $h_{ij}/a_{\phi_{ij}}$ term(s) in a variogram model is equivalent to using a transformed variogram model having range 1. However, h'_{ij} is, itself, a function of ϕ_{ij}. In no way are all directional models combined into a single isotropic model that has a range of 1. Implicitly, an anisotropic model is a function of both h_{ij} and ϕ_{ij} and cannot be made isotropic.

Note

In practice, the use of Equation (6) or (7) is to be preferred over that of Equation (4) because they are computationally more efficient. Sine and cosine evaluations are slow operations and the use of (4) requires at least one sine and one cosine evaluation (depending on how it is coded) for each pair of points requiring a variogram estimate. If the $\boldsymbol{R}$ matrix is permanently stored, then calculation of $a_{\phi_{ij}}$ in Equation (6) requires only one sine and one cosine evaluation. This fact may be what has lead to the use of the reduced distance concept and the resulting confusion concerning "equivalent isotropic" models. If one is simply fitting a variogram model and is not concerned with the interpretation of the model parameters, then Equation (7) is preferred, as it requires neither the translation nor the rotation of axes.

SILL ANISOTROPY

With sill anisotropy, the sill varies with direction. Clark (1980), McBratney and Webster (1986), Isaaks and Srivastava (1989), among others, indicate that sill anisotropy is not nearly as common as range anisotropy. Sill anisotropy has been dealt with in a rather *ad hoc* manner. While range anisotropy has been clearly dealt with by modeling the range as an ellipse, rather than modeling the sill directly, it is usually assumed that directionally varying sills can be accommodated by using two or more range-anisotropic structures, one with a very large anisotropy ratio.

Using a Range-Anisotropic Structure with a Large Anisotropy Ratio

The approach to fitting a sill-anisotropic variogram surface using a range-anisotropic structure with a large anisotropy ratio η can be thought of as a sequential process. The motivation for the approach is explained with the help of Figure 3. Assume, for the moment, that the variogram model displays no range anisotropy. An isotropic model that well fits the experimental variogram in the direction of minimum sill is computed. In Figure 3, this is represented in each panel by the lower of the two surfaces. The spherical model was used for both structures. The direction of minimum sill is 120° and the common range is 40. The sill in this direction is five.

Now a second structure is added to the first. The sill of the second structure is taken to be the difference between the maximum and minimum sills of the directional variograms. In the case of Figure 3, the maximum and minimum sills are eight and five, respectively. The minimum range in the second structure is 40 and the maximum is set to a very large value. In Figure 3 the anisotropy ratio was set to 1000 so the maximum range was 40,000.

If we look at the form of the spherical model the reasoning for using the elongated range ellipse approach to sill modelling becomes clear. Dropping the ij

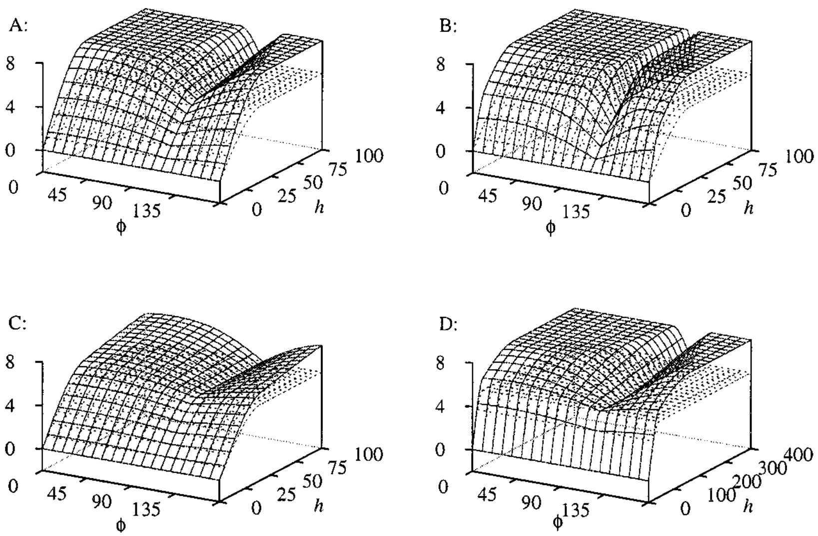

Figure 3. Variogram surfaces displaying sill anisotropy modeled using the ellongated ellipse approace. Parameters for the first structure, all four panels, are $c_1 = 5$, $a_1 = 40$, and $\eta_1 = 1$. Parameters for the second structure are $c_2 = 3$, $\theta_2 = 120°$, $\eta_2 = 1000$, and A, $a_2 = 40$, B, $a_2 = 10$, C, $a_2 = 80$, D, $a_2 = 80$.

subscripting used in the previous section, the range-anisotropic spherical model takes the form $2\gamma(h,\phi) = c(1.5h/a_\phi - 0.5(h/a_\phi)^3)$ where, as before, a_ϕ is the range in direction a_ϕ. There will be a maximum lag distance that any application will use. It will be determined by either the boundaries of the geographical region under consideration or by the size of the window used for kriging, or both. In panels A–C, it is assumed to be 100. As ϕ approaches the direction of minimum sill for the second structure, which is also the direction of maximum range, the denominator in the h/a_ϕ terms becomes very large and $h/a_\phi \to 0$. Thus the contribution of the second structure, in the direction of minimum sill, is negligible. It is largest in the direction of maximum sill. The overall model for Figure 3A is

$$2\gamma(h,\phi) = 5(1.5(h/40) - 0.5(h/40)^3) + 3(1.5(h/a_\phi) - 0.5(h/a_\phi)^3)$$

where a_ϕ is computed as in the previous section, with $a_{\min} = 40$ and $\eta = 1000$.

We began the description of this example with the assumption that the underlying variogram model is not range-isotropic. From Figure 3A, it is apparent that for angles of about 0–80, and at 120, the range seems to be close to 40. From about 0 to 80 the sill is constant at 8. The range in directions 80–170 is significantly different from 40 and the sills appear to change with direction. In fact, by the very act of using a range-anisotropic second structure, the range changes continuously from 40 to 40,000 and the sill is constant at 8. This is not an argument against the use of range-anisotropic structures as models of sill-anisotropic processes providing the fitted variogram fits the experimental variogram well in all directions over the range of experimental data.

Figures 3B and C differ from Figure 3A only in the value used for the minimum range of the second structure. For Figure 3B it was set to 10 and in Figure 3C it was 80. The variogram surface in Figure 3C is generally smooth throughout except for the bend at the range of the first structure and for the crease in the direction of minimum sill. Indeed, models of this form always produce a crease in the direction of minimum sill. Figure 3D is identical to Figure 3C except that the length of the lag distance axis was increased to 400 to better indicate the constant sill and the crease in the direction of the minimum sill.

Modeling the Sill as an Ellipse

The elongated ellipse procedure, just described, has become the standard for fitting variogram models to experimental variograms exhibiting directionally varying sills. Sill-anisotropic variograms, alternatively, can be fitted using the same procedure used to model range anisotropy.

Let $c_{\max}$ be the maximum sill, $c_{\min}$ be the minimum sill, $\nu = c_{\min}/c_{\max}$ be the sill anisotropy ratio, and θ_c be the direction of maximum sill. Then the sill in direction ϕ can be modeled as an ellipse using

$$\begin{aligned} c_\phi &= c_{\max}\nu/\sqrt{\nu^2\cos^2(\phi-\theta_c)+\sin^2(\phi-\theta_c)} \\ &= \sqrt{u_\phi^2+v_\phi^2} = h\cdot c_{\max}c_{\min}/\sqrt{(c_{\min}u)^2+(c_{\max}v)^2} \\ &= h/\sqrt{b_1\Delta x^2 - b_2\Delta x\Delta y + b_3\Delta y^2} \end{aligned}$$

where

$$\begin{bmatrix} u \\ v \end{bmatrix} = \begin{bmatrix} \cos\theta_c & \sin\theta_c \\ -\sin\theta_c & \cos\theta_c \end{bmatrix} \begin{bmatrix} \Delta x_{ij} \\ \Delta y_{ij} \end{bmatrix}$$

and

$$\begin{aligned} b_1 &= (\cos\theta_c/c_{\max})^2 + (\sin\theta_c/c_{\min})^2 \\ b_2 &= 2\sin\theta_c\cos\theta_c\left(1\big/c_{\min}^2 - 1\big/c_{\max}^2\right) \\ b_3 &= (\sin\theta_c/c_{\max})^2 + (\cos\theta_c/c_{\min})^2 \end{aligned}$$

As an example, Figure 1A was generated by plotting

$$2\gamma(h,\phi) = (3/\sqrt{(3/8)^2\cos^2(\phi-30)+\sin^2(\phi-30)})(1.5(h/100)-0.5(h/100)^3)$$

for different values of h and ϕ. Indeed, any directionally varying parameter, whether it be the range, sill, slope, nugget, or whatever, can be modeled using this approach provided that the assumption that the directionally changing parameters lie approximately on an ellipse is reasonable.

Zimmerman (1993) expressed concern regarding the use of sill-anisotropic models because they are not second-order stationary. The question of sill-anisotropy and stationarity will be addressed in another paper.

POWER MODELS

As usually written, the power model has the form $2\gamma(h) = ch^a$, where $0 < a < 2$. As just noted, either or both of the parameters in this model can be modeled as an ellipse yielding, for example,

$$2\gamma(h,\phi) = c_\phi h^{a_\phi} \tag{9}$$

Pannatier (1996) and Deutsch and Journel (1998) both state that their software handles anisotropy in the correct manner by calculating an anisotropic distance and leaving the parameter a unchanged. Examination of the GSLIB code, however, and empirical experience with VARIOWIN-fitted models reveals that, in the case of $\eta < 1$, both programs use the equation

$$2\gamma(h, \phi) = c'_{\max}(h')^a = c'_{\max}(c'_{\max}/c'_{\phi})^a h^a$$

where

$$c'_{\phi} = c'_{\max}c'_{\min} \Big/ \sqrt{c'^2_{\min}\cos^2(\phi - \theta') + c'^2_{\max}\sin^2(\phi - \theta')} \tag{10}$$

is an elliptically varying parameter. This is because these programs compute h' as $\sqrt{u'^2 + (v'/\eta')^2}$. The result follows from Equation (6). The meaning of the primes will be made clear in a moment. No other programs were checked, but we suspect that this usage is common. There is nothing inherently wrong with this model since $c_{\text{common},\phi} = c'_{\max}(c'_{\max}/c'_{\phi})^a$ can be considered a model for the anisotropic slope parameter. However, there is no reason to believe that the slope parameter, $c_{\text{common},\phi}$ in this case, should be related to the power parameter a. Plotted in Figure 4 is the the shape formed by $c_{\text{common},\phi}$, as ϕ varies from 0° to 360°, for the case of $c'_{\max} = 15$, $c'_{\min} = 9.402$, $a = 1.99$, and $\theta' = 135°$. Also plotted is an ellipse having identical major and minor axes.

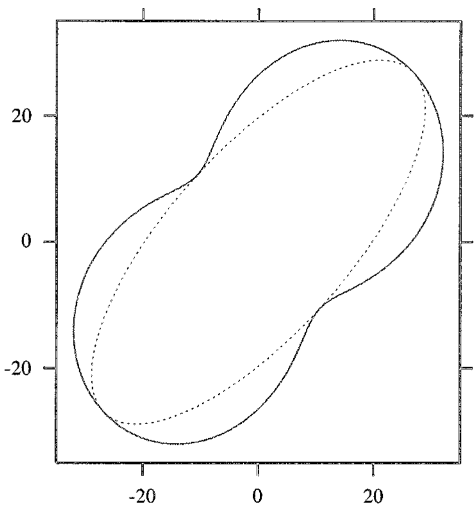

Figure 4. Shape generated from the directionally varying slope parameter of a power model used by Cressie (1991) and implemented in GSLIB (1998) and VARIOWIN (1996), together with an ellipse having identical major and minor axes. The parameters used are Cressie's.

Cressie (1989, 1991, p. 217) also "miscalculated" the power model in this way, though he stated the model as $\hat{c}_0 + c_{\text{cres},\phi} h^a$, where $\hat{c}_0$ is a nugget structure and

$$c_{\text{cres},\phi} = \left(c_{\max}^{2/a} \cos^2(\pi/4 - \phi) + c_{\min}^{2/a} \cos^2(\pi/4 + \phi)\right)^{a/2}$$

for the particular case of $\theta = \pi/4$. To fully understand the meanings of parameter values that one must supply to `GSLIB` or `VARIOWIN`, it is instructive to establish the relationship between the `VARIOWIN`-like parameterization and Cressie's.

To establish the equivalence between $c_{\text{common},\phi}$ and $c_{\text{cres},\phi}$, simply substitute the definition (10) of the elliptically varying parameter c'_ϕ into $c_{\text{common},\phi} = c'_{\max}(c'_{\max}/c'_\phi)^a$. After a little algebra, one finds that

$$\begin{aligned}
c_{\text{common},\phi} &= \left(c'^{\,2/a}_{\max} \cos^2(\phi - \theta') + \left(c'_{\max}\left(\frac{c'_{\max}}{c'_{\min}}\right)^a\right)^{2/a} \sin^2(\phi - \theta')\right)^{a/2} \\
&= \left(c'^{\,2/a}_{\max} \cos^2(\theta' - \phi) + \left(c'_{\max}\left(\frac{c'_{\max}}{c'_{\min}}\right)^a\right)^{2/a} \sin^2(\theta' - \phi)\right)^{a/2} \\
&= \left(\left(c'_{\max}\left(\frac{c'_{\max}}{c'_{\min}}\right)^a\right)^{2/a} \cos^2\left(\left(\theta' \pm \frac{\pi}{2}\right) - \phi\right)\right. \\
&\quad \left. + c'^{\,2/a}_{\max} \sin^2\left(\left(\theta' \pm \frac{\pi}{2}\right) - \phi\right)\right)^{a/2}
\end{aligned}$$

This is the general form for the equivalence of the two parameterizations. It is now clear that $c'_{\max} = c_{\min}$, $c'_{\min} = c_{\min}(c_{\min}/c_{\max})^{1/a}$ and that $\theta' = \theta \pm \pi/2$. In Cressie's particular example $\theta = \pi/4$, in which case it is also true that $\sin^2(\theta - \phi) = \cos^2(\theta + \phi)$. The reason $\theta' = \theta \pm \pi/2$ is that the direction of maximum c'_ϕ is the direction of minimum c_ϕ. That is, because $c'_{\max} = c_{\min}$.

In Cressie's example, $c_{\max} = 38$, $c_{\min} = 15$, and $\theta = 45$. Therefore $\eta = 0.395$, $c'_{\max} = 15$, $c'_{\min} = 9.402$, and $\eta' = 0.627$. Notice that $\eta' = \eta^{1/a}$. The primed values, θ', $c'_{\max}$, and η', are those that one would provide to `VARIOWIN` or to `GSLIB` in order to duplicate Cressie's example. Figure 5 compares the resulting variogram surface (panel A) obtained using Cressie's parameters with that obtained using an elliptically changing slope parameter $2\gamma(h, \phi) = c_\phi h^a$ (panel B).

When `GSLIB` or `VARIOWIN` are used with a spherical, exponential, or Gaussian model, one obtains identical fits by specifying either the maximum of the directionally changing parameters, the direction θ of this maximum parameter, and an anisotropy ratio η less than one, or by specifying the minimum of the directionally changing parameters, the direction, $\theta \pm \pi/2$ of this minimum, and an anisotropy ratio $1/\eta$ greater than one. This is not true with the power model. If one were

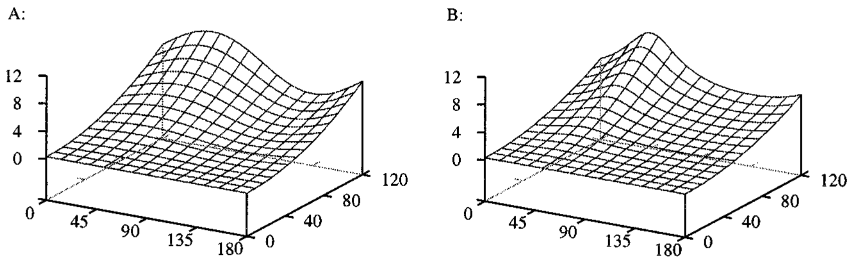

Figure 5. Panel A is Cressie's (1991) variogram surface; panel B is the surface generated using a power model with identical parameters but allowing the slope to vary along an ellipse.

to specify a power model with a slope parameter of 9.402 in direction 45 and with an anisotropy ratio of 1.595, one would not replicate Cressie's variogram model.

In the case of $\eta > 1$ the roles of $c_{\max}$ and $c_{\min}$ are switched throughout. A development similar to that above reveals that for $\eta > 1$, $c'_{\min} = c_{\max}$ and $c'_{\max} = c_{\max}(c_{\max}/c_{\min})^{1/a}$. As in the $\eta < 1$ case, when η is greater than one $\theta' = \theta \pm \pi/2$ and $\eta' = \eta^{1/a}$. In order to replicate Cressie's Figure 4.3 in using an anisotropy ratio greater than one in `VARIOWIN`, one would need to specify the "minimum" power of 38, not 9.402.

PUTTING IT TO WORK

`VARIOWIN` (Pannatier, 1996) allows the user to interactively tweak variogram parameters and to simultaneously view the changes in multiple directions (different ϕ's). However, because `VARIOWIN`'s maximum zoom level is fixed at the screen size, it is difficult to view the results in more than four directions at any one time. With highly anisotropic models, this is a limitation. In this section we will demonstrate how `VARIOWIN` was used in combination with weighted nonlinear regression to fit a variogram surface for a random function of elevation using the ellipse-based approach for both range and sill anisotropies.

The data for this example are elevations obtained from topographic maps in an area somewhat larger than a USGS quadrangle in southwestern Texas. The "variogram surface" option of `VARIOWIN` (Figure 6) was used to determine the approximate angles of anisotropy. There appears to be three directions of anisotropy: one at about 20, one at about 70°, and a third at about 100°. A fourth direction was at about 85° was identified by some of the fitted models. Twelve experimental variograms were fitted from 0° to 165° at 15° intervals with an angular tolerance of 7.5°and a lag distance of 200 m to a maximum separation of 8000 m. While viewing the experimental variograms in directions 0°, 45°, 90°, and 135°, `VARIOWIN` was then used to fit a directional variogram consisting of two range-anisotropic

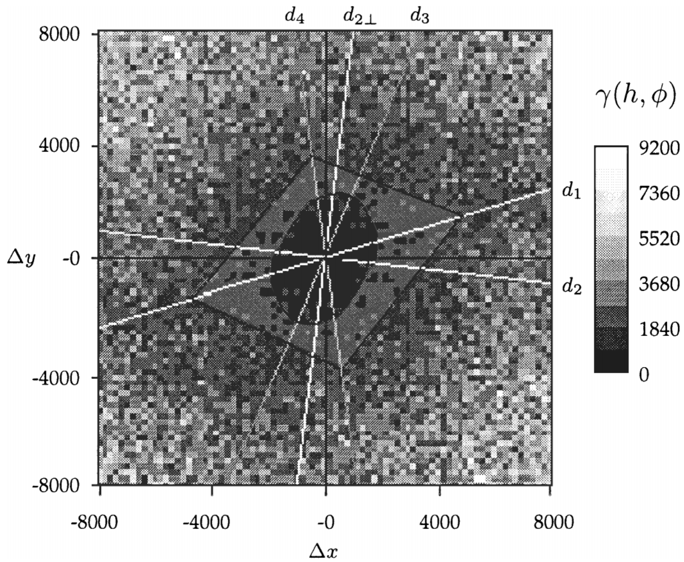

Figure 6. Variogram surface from `VARIOWIN` with directions and general shapes of anisotropy identified. The particular directions d_1 and d_4 are those identified by the model in Figure 7E. They define the central rhombus of moderate variogram values. d_2 and $d_{2\perp}$ define the central ellipse of low variogram values. Some models hinted of another axis in direction d_3.

structures: $2\gamma(h, \phi) = c_1\text{Sphr}(a_{1\phi}) + c_2\text{Sphr}(a_{2\phi})$. This is an eight-parameter model. The second structure had an anisotropy ratio of 1000, the maximum allowed by `VARIOWIN`, indicating a sill-anisotropic variogram surface.

The parameters obtained from `VARIOWIN` were then used as starting values for the weighted nonlinear regression using the experimental variogram values in all 12 directions. Iteratively reweighted least squares was used with weights equal to $N(h, \phi)/\gamma(h, \phi)^2)$, where $N(h, \phi)$ is the number of data values used to calculate a particular experimental value, as suggested, for example, by Cressie (1991).

Figure 7 shows the resulting variogram surfaces. Panel A shows the result of fitting a single range-anisotropic structure, $2\gamma_a(h, \phi) = c_1\text{Sphr}(a_{1\phi})$, to the experimental variogram values of the elevation data. Panel B shows a single sill-anisotropic structure, $2\gamma_b(h, \phi) = c_{1\phi}\text{Sphr}(a_1)$. The similarity of the two surfaces is a result of the fact that the minimum range in panel A and the range in panel B are both well beyond the maximum lag value displayed, and neither fitted surface had an elongated ellipse. These are both four-parameter models. The model used for panel C specified that both structures were sill-isotropic and range-anisotropic. The fitted model (Table 1) indicated that one of the structures

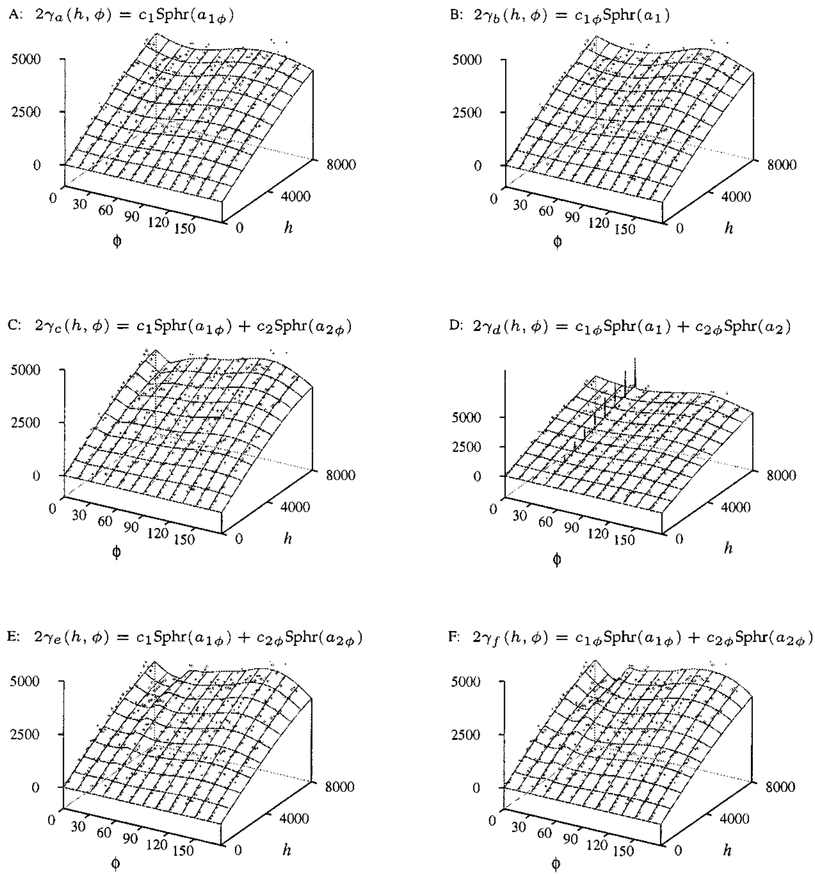

Figure 7. Variogram surface fitted to experimental variogram values from elevation data. A: $2\gamma_a(h,\phi) = c_1\mathrm{Sphr}(a_{1\phi})$; B: $2\gamma_b(h,\phi) = c_{1\phi}\mathrm{Sphr}(a_1)$; C: $2\gamma_c(h,\phi) = c_1\mathrm{Sphr}(a_{1\phi}) + c_2\mathrm{Sphr}(a_{2\phi})$; D: $2\gamma_d(h,\phi) = c_{1\phi}\mathrm{Sphr}(a_1) + c_{2\phi}\mathrm{Sphr}(a_2)$; E: $2\gamma_e(h,\phi) = c_1\mathrm{Sphr}(a_{1\phi}) + c_{2\phi}\mathrm{Sphr}(a_{2\phi})$; F: $2\gamma_f(h,\phi) = c_{1\phi}\mathrm{Sphr}(a_{1\phi}) + c_{2\phi}\mathrm{Sphr}(a_{2\phi})$.

has a very elongated range-ellipse at about 17°, possibly indicating sill-anisotropy. While not pronounced in this case, the crease in surface C is characteristic of the elongated ellipse approach to modeling sill anisotropy.

Panel D shows the fitted surface for a two-structure model $2\gamma_d(h,\phi) = c_{1\phi}\mathrm{Sphr}(a_1) + c_{2\phi}\mathrm{Sphr}(a_2)$, with both structures range-isotropic and sill-anisotropic. Not only does this eight-parameter model have a larger residual sum of squares compared to the eight-parameter model, C, the spike at 45° is unacceptable. Such spikes result from very elongated c_ϕ-ellipses much like the elongated

Table 1. Parameter Estimates and Half-Widths of the 68.3% Confidence Intervals About the Estimates for Variogram Surfaces Fitted to the Experimental Elevation Variogram Values

Model	Parameter	Estimate	Half-width
A:	$2\gamma_a(h,\phi) = c_1\mathrm{Sphr}(a_{1\phi})$:	$\sigma^2 = 3.477$	
	$a_{\max 1}$	15,559.9	1124.0
	$a_{\min 1}$	11,633.9	893.8
	θ_{a1}	39.3	2.0
	c_1	4104.7	267.7
B:	$2\gamma_b(h,\phi) = c_{1\phi}\mathrm{Sphr}(a_1)$:	$\sigma^2 = 3.273$	
	a_1	12,097.6	745.3
	$c_{\max 1}$	4371.7	235.7
	$c_{\min 1}$	3320.1	176.9
	θ_{c1}	130.5	1.8
C:	$2\gamma_c(h,\phi) = c_1\mathrm{Sphr}(a_{1\phi}) + c_2\mathrm{Sphr}(a_{2\phi})$:	$\sigma^2 = 3.156$	
	$a_{\max 1}$	$1.10\mathrm{e}+06$	26,640.0
	$a_{\min 1}$	23,041.5	$9.4\mathrm{e}+06$
	θ_{a1}	16.8	2.1
	c_1	3025.5	3187.0
	$a_{\max 2}$	14,673.2	1476.0
	$a_{\min 2}$	9022.6	561.8
	θ_{a2}	83.4	4.2
	c_2	2534.1	189.5
D:	$2\gamma_d(h,\phi) = c_{1\phi}\mathrm{Sphr}(a_1) + c_{2\phi}\mathrm{Sphr}(a_2)$:	$\sigma^2 = 3.214$	
	a_1	12,638.2	899.3
	$c_{\max 1}$	4576.3	288.6
	$c_{\min 1}$	3411.4	242.5
	θ_{c1}	130.6	1.8
	a_2	21748.7	203,500.0
	$c_{\max 2}$	7767.9	$1.55\mathrm{e}+09$
	$c_{\min 2}$	1.8	60.5
	θ_{c2}	45.2	204.3
E:	$2\gamma_e(h,\phi) = c_1\mathrm{Sphr}(a_{1\phi}) + c_{2\phi}\mathrm{Sphr}(a_{2\phi})$:	$\sigma^2 = 2.921$	
	$a_{\max 1}$	226,714	376,800.0
	$a_{\min 1}$	13,275.4	1847.0
	θ_{a1}	30.5	2.5
	c_1	4225.6	522.9
	$a_{\max 2}$	35,320.7	$2.716\mathrm{e}+4$
	$a_{\min 2}$	7465.3	451.0
	θ_{a2}	100.0	4.2
	$c_{\max 2}$	2311.5	302.6
	$c_{\min 2}$	647.7	62.9
	θ_{c2}	35.0	3.0
F:	$2\gamma_f(h,\phi) = c_{1\phi}\mathrm{Sphr}(a_{1\phi}) + c_{2\phi}\mathrm{Sphr}(a_{2\phi})$:	$\sigma^2 = 2.877$	
	$a_{\max 1}$	228,799.0	$7.41\mathrm{e}+5$
	$a_{\min 1}$	14,530.2	2695.0
	θ_{a1}	29.4	4.2
	$c_{\max 1}$	6038.9	1390.0
	$c_{\min 1}$	4444.1	706.5
	θ_{c1}	27.2	12.91
	$a_{\max 2}$	27,304.6	$2.88\mathrm{e}+4$
	$a_{\min 2}$	6669.7	932.5
	θ_{a2}	88.3	6.6
	$c_{\max 2}$	2276.5	798.4
	$c_{\min 2}$	476.2	131.3
	θ_{c2}	34.7	4.6

a_ϕ-ellipses produce creases in variogram surfaces. In the case of the elevation data, it resulted from the fact that the experimental variograms in directions 45° and 60° were both slightly above the first variogram structure. Other starting values used for $2\gamma_d(h, \phi)$ resulted in local minima having shapes very similar to Figure 7B. The estimated parameters for the second structure of these models were not significantly different from zero, indicating that $2\gamma_b(h, \phi)$ is preferred over $2\gamma_d(h, \phi)$.

To further investigate the flexibility of using the ellipse-approach to variogram surface modeling, both the sill and the range parameters were allowed to vary along ellipses. The two-structure model $2\gamma_e(h, \phi) = c_1 \text{Sphr}(a_{1\phi}) + c_{2\phi} \text{Sphr}(a_{2\phi})$ (panel E) was fitted. This is a ten-parameter model having an elongated range-ellipse in direction $\theta_{a2} = 30°$, as evidenced by the surface crease in this direction. The twelve-parameter model, $2\gamma_f(h, \phi) = c_{1\phi} \text{Sphr}(a_{1\phi}) + c_{2\phi} \text{Sphr}(a_{2\phi})$ (panel F) was also fitted. It, too, has an elongated range-ellipse in direction $\theta_{a1} = 30°$. With the exception of the maximum range of the elongated ellipses, all parameters in both of these models are significantly different from zero. The lack of significance of the maximum range is typical of elongated ellipses. Since the maximum range occurs well beyond the maximum lag in the data, it is difficult, at best, to tie down. Indeed, if it is really assumed to approach infinity, then it would be impossible to estimate. It is, however, needed in the model in order to define an anisotropy ellipse.

Model $2\gamma_e(h, \phi)$ identified significant anisotropies in directions $\theta_{a1} = 30°$, $\theta_{a2} = 100°$, $\theta_{c2} = 35°$. Those at 30° and 100° are generally consistent with the directions that were *a priori* expected based on the `VARIOWIN` surface (Fig. 6). In particular, they identify the axes d_1 and d_4 of the central rhombus comprised of variogram values near 2000. The maximum sill at 35° is harder to explain based on the `VARIOWIN` surface plot. From the variogram surface plot (Fig. 7E) it is clearly the direction at which the surface levels out after the dip centered at about 30°. Some fitted equations hinted at anisotropies at about 70° (d_3) and at about 85° ($d_{2\perp}$). These directions were not identified by the fitted Model E nor was the central ellipse (Fig. 6) having variogram values near 1000.

Some authors, e.g., Isaaks and Srivastava (1989), have argued against over-fitting the variogram models. Because Kriging depends so heavily on the variogram model assumed, we disagree to the extent that the amount of data used to compute the experimental variogram values is sufficient. In the case of the elevation data, even at the largest lags there were approximately 250 pairs of points used to compute the experimental values. In our case, the maximum size of the Kriging windows that were used was about 4000 m. With the exception of $2\gamma_d(h, \phi)$, all of the above models are acceptable for this size of window. Model $2\gamma_e(h, \phi)$ has the about the same residual variance as the full model and a slightly lower approximate Akaike Information Criteria value; it would be preferred for kriging windows approaching 8000 m in radius.

SUMMARY AND CONCLUSIONS

We have attempted to demystify the computations required for sill and range anisotropic variogram models. In so doing, we have provided the equations necessary to model any parameter, not just the range, as directionally varying on an ellipse. We have noted that, while not "incorrect," they are after all models, some published models do not coincide with the verbiage used to describe them. At least some implementations of the power model confound the computation of the slope parameter with that of the power parameter. The slope parameter computed using commonly available software for power models does not vary along an ellipse. Finally, if sampling is dense enough, we advocate calculating experimental variogram values for more than four directions and using weighted nonlinear regression or some other, related technique (e.g., Cressie, 1985; McBratney and Webster, 1986; Vecchia, 1988), for model fitting and displaying the fitted surface together with the experimental variogram values in as many directions as is reasonable.

REFERENCES

Clark, I., 1980, Part 2: The semivarigram, *in* Royle, A., Clark, I., Brooker, P. I., Parker, H., Journel, A., Rendu, J. M., Sandefur, R., Grant, D. C., and Mousset Jones, P., Geostatistics: McGraw Hill, New York, p. 29–40.

Cressie, N. A. C., 1985, Fitting variogram models by weighted least squares: Math. Geology, v. 17, no. 5, p. 563–586.

Cressie, N. A. C., 1989, Geostatistics: Am. Statistician, v. 43, no. 4, p. 197–202.

Cressie, N. A. C., 1991, Statistics for Spatial Data: John Wiley & Sons, New York, 900 p.

Deutsch, C. V., and Journel, A. G., 1998, GSLIB: geostatistical software library and user's guide: 2nd Ed.: Oxford University Press, New York, 369 p.

Goovaerts, P., 1997, Geostatistics for natural resources evaluation: Oxford University Press, New York, 483 p.

Isaaks, E. H., and Srivastava, R. M., 1989, An introduction to applied statistics: Oxford University Press, New York, 561 p.

Journel, A. G., and Huijbregts, C. J., 1978, Mining geostatistics: Academic Press, New York, 600 p.

McBratney, A. B., and Webster, R., 1986, Choosing functions for semi-variograms of soil properties and fitting them to sampling estimates: Jour. Soil Sci., v. 37, no. 4, p. 617–639.

Myers, J. C., 1997, Geostatistical error management: Quantifying uncertainty for environmental sampling and mapping: Van Nostrand Reinhold, New York, 571 p.

Pannatier, Y., 1996, VARIOWIN software for spatial data analysis in 2D: Springer-Verlag, New York, 91 p.

Vecchia, A. V., 1988, Estimation and model identification for continuous spatial processes: Jour. Royal Stat. Assoc., Series B, v. 50, no. 2, p. 297–312.

Zimmerman, D. L., 1993, Another look at anisotropy in geostatistcs: Math. Geology, v. 25, no. 4, p. 453–470.